Hole diffusion effect on the minority trap detection and non-ideal behavior of $NiO/\beta\text{-}Ga_2O_3$ heterojunction

Madani Labed[1,2,] *, Saud Alotaibi[3,4], Ji Young Min[1,2], Abdulaziz Almalki[4,5], Mohamed Henini[4,*] and You Seung Rim[1,2,]*,

[1]Department of Intelligent Mechatronics Engineering and Convergence Engineering for Intelligent Drone, Sejong University, Seoul 05006, Republic of Korea

[2]Department of Semiconductor Systems Engineering and Institute of Semiconductor and System IC, Sejong University Seoul 05006, Republic of Korea

[3]Physics Department, Faculty of Science and Humanities in Ad-Dawadmi, Shaqra University, 11911, Saudi Arabia

[4]School of Physics and Astronomy, University of Nottingham, Nottingham NG7 2RD, UK

[5]Physics Department, Faculty of Science at Taibah University-Yanbu, King Khalid Rd. Al Amoedi, 46423, Yanbu El-Bahr, 51000, Saudi Arabia

* Corresponding authors:

E-mail: madani@sejong.ac.kr (M.L) youseung@sejong.ac.kr (Y.S. Rim) and Mohamed.Henini@nottingham.ac.uk (M. H)

Abstract

A $NiO/\beta\text{-}Ga_2O_3$ heterojunction was fabricated by sputtering a highly p-doped NiO layer onto $\beta\text{-}Ga_2O_3$. This heterojunction showed a low leakage current and a high turn-on voltage (V_{on}) compared to a $Ni/\beta\text{-}Ga_2O_3$ Schottky barrier diode. The extracted V_{on} from the $NiO/\beta\text{-}Ga_2O_3$ heterojunction's forward current-voltage characteristics was ~1.64 V, which was lower than the extracted built-in potential voltage (V_{bi}) obtained from the capacitance-voltage curve. To explain this difference, deep level transient spectroscopy and Laplace-deep level transient spectroscopy

were employed to study majority and minority traps in β-Ga_2O_3 films. A new minority trap was detected near the surface of β-Ga_2O_3 under a reverse bias of -1 V but wasn't observed at -4 V, indicating its dependence on hole injection density. Using Silvaco TCAD, the hole diffusion length from P+-NiO to β-Ga_2O_3 was determined to be 0.15 μm in equilibrium, which is increased with increasing forward voltage. This finding explained why the trap level wasn't detected at a large reverse bias. Moreover, hole diffusion from NiO into β-Ga_2O_3 significantly affected the β-Ga_2O_3 surface band bending and impacted transport mechanisms. It was noted that the energy difference between the conduction band minimum (CBM) of β-Ga_2O_3 and the valence band maximum (VBM) of NiO was reduced to 1.60 eV, which closely matched the extracted Von value. This supported the dominance of direct band-to-band tunneling of electrons from the CBM of β-Ga_2O_3 to the VBM of NiO under forward bias voltage.

Keywords: β-Ga_2O_3, NiO, DLTS, Traps, minority carrier, V_{on}, D-BBT, TAT, Modeling.

Gallium Oxide (Ga_2O_3) is an ultrawide-bandgap semiconductor material with unique properties that make it highly attractive for a range of electronic and optoelectronic applications[1]. Ga_2O_3 exhibits excellent electrical and optical characteristics especially the beta (β) phase[2]. β-Ga_2O_3 possesses a wide bandgap, typically in the range of 4-5 eV[3]. This large bandgap allows β-Ga_2O_3 to have excellent electrical and optical properties, making it suitable for harsh operating conditions such as high-power, high frequency and high-temperature applications[4,5]. Its ultrawide bandgap and high breakdown electric field also enables β-Ga_2O_3-based devices to operate at high voltages and high temperatures making them well-suited for power electronics and high-voltage applications[6]. In addition, β-Ga_2O_3 also demonstrates good thermal stability and chemical durability[7]. This makes β-Ga2O3 suitable for applications in solar cells[8], light-emitting diodes

(LEDs)[9], solar blind photodetectors[10,11], MOSFET[12,13] and other electronic devices. However, the development of stable and efficient p-type β-Ga_2O_3 is still a complex and unresolved issue [14] because of the very high hole effective mass which affect the hole density and hole mobility in β-Ga_2O_3[1]. It is important to note that other P-type semiconductors such as NiO are found to be useful for the development of bipolar devices such as field effect transistors [15,16]. Further improvements in β-Ga_2O_3 based devices were demonstrated for example by Zhou et al. [17] who demonstrated a NiO/β-Ga_2O_3 heterojunction architecture with high avalanche and surge current robustness, minimal reverse recovery, as well as an excellent trade-off between on-resistance and breakdown voltage. These properties are considered a great step forward towards the next generation of power semiconductor devices. However, to gain a deeper understanding and successfully integrate semiconductor physics with advanced characterization techniques, further efforts are essential to enhance the performance and stability of β-Ga_2O_3 devices. Among the range of characterization techniques available, deep level transient spectroscopy (DLTS) stands out as a valuable tool. DLTS plays a crucial role in unraveling the intricate device physics of β-Ga_2O_3, paving the way for even greater achievements in this field

However, the low hole density and mobility of minority carriers makes the detection of electrically active minority trap levels in β-Ga_2O_3 using deep level transient spectroscopy (DLTS) very challenging[3,18]. In this context, different techniques were proposed, and one of the easiest technique[18] is the deposition of a heterojunction (HJ) with high hole density layer (P^+-NiO) to increase the minority carrier density at the surface of β-Ga_2O_3 by the hole injection mechanism. This approach will help to detect the minority traps at the surface of β-Ga_2O_3. Although the hole injection plays a crucial role for increasing the minority carriers in β-Ga_2O_3, however, this injection will affect the interface band alignment, transport mechanism and also

the HJ parameters. Among these impacted parameters is the turn-on voltage (V_{on}) value, which is much lower than the built-in potential value (V_{bi}) as reported previously. The first expected reason for this difference is explained by the tunneling of electrons from the CBM of β-Ga_2O_3 into the VBM of p-NiO, which is mediated by majorities trap states[18–20]. The effect of the inhomogeneity of the barrier height of the NiO/β-Ga_2O_3 heterojunction was also considered by Wang el al.[21].

In this context, the role and the effect of hole injection from P^+-NiO fabricated using radio frequency (RF) sputtering to the surface of β-Ga_2O_3 for improving the detection of minority traps at the surface of β-Ga_2O_3 were studied using DLTS, Laplace-DLTS (LDLTS) and Silvaco TCAD simulator. Furthermore, the dominant transport mechanisms were investigated in order to understand the reason for the difference between turn-on voltage (V_{on}) and build-in potential (V_{bi}) values.

Here, the fabricated Schottky barrier diodes (SBD) and NiO/β-Ga_2O_3 heterojunctions (HJ) were fabricated on a Si-doped β-Ga_2O_3 epitaxial layer deposited on a Sn-doped β-Ga_2O_3 single crystal wafer (415 μm thick, N_d-$N_a \approx 10^{18}/cm^3$) purchased from Novel Crystal Technology, Inc. Before depositing NiO and Ni layers, the surface of the Si-doped β-Ga_2O_3 was cleaned using chemical and mechanical polishing to ensure a high-quality surface. The samples were then subjected to ultrasonic treatment with acetone and isopropanol for 15 minutes, followed by drying with N_2 gas. On the backside of the Sn-doped β-Ga_2O_3 wafer, a bilayer of Ti/Au (20 nm/80 nm thick) was evaporated using electron beam and thermal evaporation, respectively. For both HJ and SBD, radio frequency sputtering (RF sputtering) was used to deposit NiO and Ni with thicknesses of 300 nm and 100 nm, respectively, using Ni and NiO targets rerspectively with sputtering power of 30W, and the working pressure was maintained at 3 mTorr.

Subsequently, for optimizing the device, annealing was performed at 400°C in an Ar atmosphere for 1 minute. A schematic of the SBD and HJ devices is presented in **Figure 1(a)** and the SEM image of NiO/β-Ga_2O_3 HJ is shown in **Figure 1(b).**

.

Current density–voltage (J–V) and capacitance–voltage (C–V) characteristics were measured at room temperature (RT) using a Keithley 2410 source meter and Hewlett Packard 4284A LCR meter. DLTS and LDLTS were conducted for both Ni/β-Ga_2O_3 SBD and NiO/β-Ga_2O_3 HJ, where the transient capacitance was monitored by a Boonton 7200 capacitance meter during the temperature scan by applying a train of electrical pulses to the sample with a chosen filling pulse (V_P) value generated by an interface card from National Instruments. The change in capacitance transient is monitored by a computer in the form of a DLTS signal as a function of temperature.

Furthermore, Silvaco TCAD, a powerful device simulator, was used to extract the hole density profile and hole injection into the surface of β-Ga_2O_3, and to study the dominant transport mechanisms. Silvaco TCAD solves the basic drift-diffusion semiconductor equations, Poisson and continuity equations by considering different transport mechanisms such as thermionic, tunneling, direct-band to band tunneling (D-BBT) and trap-assisted tunneling (TAT). In addition, other physical models such as Shockley-Red-Hall (SRH), Auger recombination and mobility dependent electric field are considered in this simulation.

Figure 1(c) shows the semi-logarithmic J–V characteristics of NiO/β-Ga_2O_3 HJ and Ni/β-Ga_2O_3 SBD. As can be seen in **Figure 1(c)**, the HJ exhibits a low leakage current compared with SBD. Furthermore, the forward current of NiO/β-Ga_2O_3 HJ shows a kink in low forward voltage

region in contrast with Ni/β-Ga_2O_3 SBD, which is consistent with the dependence of the extracted ideality factor as a function of the applied bias (V) as evidenced in the inset of **Figure 1(c)**. For NiO/β-Ga_2O_3 HJ, as the forward bias voltage increases, the ideality factor increases and reaches a peak value 17 at 0.72 V and then gradually decreases. In contrast, for Ni/β-Ga_2O_3 SBD is almost constant with a value lower than two. ideality factor higher than 2 indicates the domination of new transport mechanism such as trap-assisted tunneling process[21]. In addition, the extracted value V_{on} for NiO/β-Ga_2O_3 HJ is 1.64 V, which is lower than V_{bi} value of about 1.89 V obtained from C-V characteristics (**Figure 1(d)**). This finding confirms the domination of trap-assisted SRH recombination mechanism[18,19,22]. Moreover, the extracted Schottky barrier height (SBH) for the NiO/β-Ga_2O_3 heterojunction is 0.93 eV, which is higher than that of the Ni/β-Ga_2O_3 Schottky barrier diode (0.85 eV). **Figure S1** shows the donor concentration (N_d) profile of Si-doped β-Ga_2O_3 epitaxial layers, which is extracted from C–V measurements. The average concentration N_d is found to be 1.32×10^{16} cm^{-3} for Ni/β-Ga_2O_3 Schottky barrier diode (SBD) and 1.36×10^{16} cm^{-3} for NiO/β-Ga_2O_3 heterojunction (HJ). The values of the hole density, resistivity, and hole mobility of the highly doped NiO film obtained using Hall measurement are found to be ~10^{19} cm^{-3}, 25.8 Ω·cm, and 0.029 cm^2/Vs, respectively. Nd in β-Ga_2O_3 is determined from the plots of $1/C^2$ versus reverse-bias voltage V_R as follows [23]:

$$\frac{1}{C^2} = \frac{2(V_{bi}+V_R)}{q\varepsilon_s\varepsilon_0 N_d} \quad (1)$$

Here, V_R is the reverse-bias voltage, V_{bi} is the build-in- potential, N_d is the donor doping concentration and ε_s is the permittivity of β-Ga_2O_3 ($\varepsilon_s=11\varepsilon_0$, where ε_0 is the dielectric constant of free space, which is equal to 8.85×10^{-14} F/cm) of β-Ga_2O_3. The values of N_d and V_{bi} can be determined from the slope and intercept of the $1/C^2$ curve, as indicated in equation (1).

To determine the presence of electrically active defects in both structures, namely Ni/β-Ga_2O_3 SBD and NiO/β-Ga_2O_3 HJ, and to confirm the hole injection for minority traps detection of NiO/β-Ga_2O_3 HJ DLTS measurements were carried out under identical conditions. DLTS parameters adopted in this study include a reverse bias, V_R = -1 V and -4 V, a filling pulse height, V_P = 0 V, a filling pulse time, t_P = 1 msec, and a rate window of 500 s^{-1}. In Figure 2(a), the DLTS signals have been plotted against temperature for both structures over the scanned temperature range of 10 to 450 K at V_R= -1 V. It has been found that the Ni/Ga_2O_3 SBD exhibits two electron traps. However, the NiO/β-Ga_2O_3 HJ exhibits a single electron and a hole trap as shown in Figure 2(a). Due to the broad nature of the DLTS peaks, Laplace DLTS (LDLTS) measurements were carried out in order to resolve these peaks. Using LDLTS technique, the activation energy, trap concentration, and cross section of these traps are extracted from the Arrhenius plots as shown in Figure 2(b). The activation energy, trap concentrations, and capture cross-section of these traps are summarized in Table I. As shown in Table I at -1 V, Ni/β-Ga_2O_3 SBD has two electron traps E_SBD1 and E_SBD2 with activation energies of 0.14 eV and 0.33 eV, respectively. However, for NiO/β-Ga_2O_3 HJ in addition to a majority trap level with a deeper energy level of about Ec-0.77 (E2) below the conduction band Ec and with the highest capture cross section (7.45×10^{-13} cm^{-2}), a new minority trap level (hole trap) was detected with an energy level Ev+0.11 (H1) above the valence band Ev. This detected hole trap level after inserting p^+-NiO layer is very close to the minority trap level reported by Wang et al.[18]. The H1 trap level could have an intrinsic origin such as oxygen and gallium vacancies[3,18,24]. The trap characteristics of both the Ni/β-Ga_2O_3 SBD and NiO/β-Ga_2O_3 HJ at VR = -1 V are detailed in **Table I**. Additionally, we have included a comparison with other detected majority and minority trap levels published by Wang et al.[18] in **Figure 2(b)**. For a reverse voltage V_R = -4 V which equivalent to depletion region thickness of about 0.73 μm, H1 trap level is not detected as shown in **Figures 2 (c)** and **(d).** The obtained LDLTS traps characteristics at V_R=-4 V are summarized in **Table I**. Three electron traps were detected in NiO/β-Ga_2O_3 HJ, however, only two electron traps in Ni/β-Ga_2O_3 SBD were observed.

In this work the lambda (λ) effect, which is explained below, is taken into consideration in order to determine accurately the concentrations of all traps. When a reverse voltage is applied, traps positioned near the depletion layer's edge do not release electrons or holes. The

width of the non-emission region (λ) is defined as the region where the trap energy level falls below the Fermi level in the neutral part of the depletion layer. This correction accounts for traps that are not involved in the emission processes of charge carriers (both electrons and holes) due to their specific location within the semiconductor structure which is given by [25]:

$$\lambda_n = L_D\sqrt{2\ln\left(\frac{N_d C_n}{e_n^t}\right)} \quad (2)$$

$$\lambda_p = L_D\sqrt{2\ln\left(\frac{N_d C_n}{e_p^t \ln(2)}\right)} \quad (3)$$

where $L_D = \sqrt{\varepsilon_s K_B T/ne^2}$ (K_B is the Boltzmann constant, T is the temperature, and n is the free carrier concentration, assuming that n = N_d) is the Debye length. e_n^t and e_p^t are the thermal emission rate of electrons and holes, and C_n and C_n are the capture coefficient of electrons and holes, respectively.

C_n and C_n are given by:

$$C_{n,p} = v_{th,n,p}\sigma_{n,p} \quad (4)$$

$$e_{n,p} = v_{th,n,p}\sigma_{n,p}n_i\exp(\frac{|E_t - E_i|}{K_B T}) \quad (5)$$

where $v_{th,n,p}$ and $\sigma_{n,p}$ are the thermal velocities and the electron and hole capture cross sections, respectively. For example the calculated lambda values for E_c-0.77 and E_v+0.11 trap levels for HJ are around 136.03 nm and 136.34 nm respectively.

Considering the lambda effect, the electron and hole traps densities ($\widetilde{N_t}$) are given by[25]:

$$N_t = \widetilde{N_t}(1 - \frac{\lambda_n}{w})^2 \quad (6)$$

$$N_t = \widetilde{N_t}(1 - \frac{\lambda_p}{w})^2 \quad (7)$$

where N_t is the true concentration of the electron and hole traps measured by DLTS and w is the depletion region width. The measured true concentrations for electron and hole traps are presented in **Table I.**

The main contributing shallow trap to the leakage current is determined using I-V measurements conducted at various temperatures. **Figure S2** shows the plots of reverse current in the dark versus 1000/T [26]. The primary shallow trap levels for the Ni/β-Ga_2O_3 SBD and NiO/β-Ga_2O_3 HJ samples are found to be at E_c-0.21 eV and E_c-0.22 eV, respectively.

According to Wang et al.[18] this minority trap level (H1) is a bulk trap but it is dependent on the hole injection effect. To confirm this dependence, Silvaco TCAD was used to extract the hole density profile. As shown in **Figure 3 (a),** the free hole carriers diffused from NiO to the surface of β-Ga_2O_3 with a diffusion length of about 0.15 μm with a low density. This explains the reason why this minority trap was not detected at the applied voltage of -4 V because of its very low hole density. However, we noticed that under highly positive forward bias conditions, such as +2 V, the energy band of the p-NiO_x experiences a downward shift. Consequently, holes highly diffused from P^+-NiO_x to surface of β-Ga_2O_3 with higher density compared with equilibrium as shown in **Figure 3 (b)**. **Figure 3 (c)** shows the extracted hole profiles at equilibrium and after an applied bias voltage of +2 V. As a result, these holes diffuse into the β-Ga_2O_3 layer, leading to a conductivity modulation effect [27].

This hole injection will affect the β-Ga_2O_3 surface band binding. As can be seen in **Figure 3 (c)**, because of the hole injection mechanism, the surface of β-Ga_2O_3 p-type conductivity increased and this will affect on the hole Fermi-level as shown in **Figure S3**. The distance between conduction band maximum (CBM) of β-Ga_2O_3 and valence band maximum

(VBM) of NiO is very narrow and this difference is about 1.60 eV. Therefore, different transport mechanisms are expected in addition to TAT.

As discussed before, the V_{on} value is lower than V_{bi} with a difference of about 0.25 V. To explain the reason for this discrepancy, the effect of D-BBT which occurs via the tunneling of electrons from CBM of β-Ga_2O_3 to VBM of NiO should be taken into account because of the small difference between CBM of β-Ga_2O_3 and VBM of NiO. The second probable mechanism is TAT by E2 (E_c-0.77) trap level which has the highest capture cross section. TAT mechanism is expected to capture electrons from CBM of β-Ga_2O_3 and transfer them to the VBM of NiO layer.

From **Figure 3(d)** it can be seen that, when both D-BBT and TAT mechanisms were not considered V_{on} is near to 1.95 V, which is much higher than the measured value and near to the V_{bi} value. This indicates the importance of D-BBT and ID-BBT mechanisms. TAT has also an important role for the observed kink at low forward voltage region as shown in **Figure 3 (d)**. As mentioned above the difference between CBM of surface of β-Ga_2O_3 and VBM of NiO is around ~ 1.60 eV, which is near the V_{on} value, and this will affect reaching HJ on state before reaching V_{bi} value by the D-BBT. From this result, D-BBT is expected to have an important role with TAT mechanism for reducing V_{on} as compared with V_{bi}. However, with less domination, TAT by H1 is expected to have a lesser effect because of high valence band offset between NiO and β-Ga_2O_3 and also H1 is a shallow trap level (very near to VBM of β-Ga_2O_3).

In summary, NiO/β-Ga_2O_3 heterojunction was analyzed using DLTS and LDLTS to extract the majority and minority traps in β-Ga_2O_3. With comparison with Ni/β-Ga_2O_3 SBD, a new minority trap with energy level of 0.11 eV above the valence band was detected for NiO/β-

Ga_2O_3 heterojunction. However, with increasing reverse voltage, this minority trap level was not detected. This indicates that this trap level is dependent on the diffusion length of the hole carrier from NiO to the surface of β-Ga_2O_3. To confirm this dependence the hole concentration profile was extracted using Silvaco TCAD. It was observed that the hole diffusion length in β-Ga_2O_3 is increased with increasing forward voltage. This diffusion highly affected the β-Ga_2O_3 surface band binding and reduced the energy distance between CBM of β-Ga_2O_3 and VBM of NiO to 1.60 eV which is very near to the extracted V_{on} value. This reduction between CBM of β-Ga_2O_3 and VBM of NiO affected the domination of a new transport mechanism which is direct band to band from CBM of β-Ga_2O_3 and VBM of NiO. Another important transport mechanism, namely trap-assisted tunneling mechanism, was found to be responsible for the formation of the kink in current density at low forward voltage.

Supplementary Material

Additional figures including the extracted donor density depth profiles of the NiO/β-Ga_2O_3 and Ni/β-Ga_2O_3 epitaxial layers (**Figure S1**), extracted shallow trap level from reverse current dependant temperature for both NiO/β-Ga_2O_3 and Ni/β-Ga_2O_3 (**Figure S2)** and **Figure S3** shows the equilibrium band diagram showing the dominating transport mechanisms

Authors contributions: All authors contributed equally to this work.

Acknowledgements: This work was supported by the Technology Innovation Program - (20016102, Development of 1.2 kV Gallium oxide power semiconductor devices technology and RS-2022-00144027, Development of 1.2kV-class low-loss gallium oxide transistor) funded by the Ministry of Trade, Industry & Energy MOTIE, Korea and Korea Institute for Advancement of Technology (KIAT) grant funded by the Ministry of Trade, Industry & Energy (MOTIE, Korea), (P0012451, The Competency Development Program for Industry Specialist) and Hyundai Motor Group.

References

[1] Z. Galazka, Semicond. Sci. Technol. **33**, 113001 (2018).

[2] J. Su, J. Zhang, R. Guo, Z. Lin, M. Liu, J. Zhang, J. Chang, and Y. Hao, Mater. Des. **184**, 108197 (2019).

[3] M. Labed, N. Sengouga, C. Venkata Prasad, M. Henini, and Y.S. Rim, Mater. Today Phys. **36**, 101155 (2023).

[4] W.R. Fahrner, R. Job, and M. Werner, Microsyst. Technol. **7**, 138 (2001).

[5] X. Hou, X. Zhao, Y. Zhang, Z. Zhang, Y. Liu, Y. Qin, P. Tan, C. Chen, S. Yu, M. Ding, G. Xu, Q. Hu, and S. Long, Adv. Mater. **34**, 2106923 (2022).

[6] B. Wang, M. Xiao, X. Yan, H.Y. Wong, J. Ma, K. Sasaki, H. Wang, and Y. Zhang, Appl. Phys. Lett. **115**, 263503 (2019).

[7] N. Makeswaran, J.P. Kelly, J.J. Haslam, J.T. McKeown, M.S. Ross, and C. V Ramana, ACS Omega **7**, 32816 (2022).

[8] T. Minami, Y. Nishi, and T. Miyata, Thin Solid Films **549**, 65 (2013).

[9] C.-H. Lin and C.-T. Lee, J. Lumin. **224**, 117326 (2020).

[10] D. Guo, Q. Guo, Z. Chen, Z. Wu, P. Li, and W. Tang, Mater. Today Phys. **11**, 100157 (2019).

[11] A. BenMoussa, A. Soltani, U. Schühle, K. Haenen, Y.M. Chong, W.J. Zhang, R. Dahal, J.Y. Lin, H.X. Jiang, H.A. Barkad, B. BenMoussa, D. Bolsee, C. Hermans, U. Kroth, C. Laubis, V. Mortet, J.C. De Jaeger, B. Giordanengo, M. Richter, F. Scholze, and J.F. Hochedez, Diam. Relat. Mater. **18**, 860 (2009).

[12] M.H. Wong, A. Takeyama, T. Makino, T. Ohshima, K. Sasaki, A. Kuramata, S. Yamakoshi, and M. Higashiwaki, Appl. Phys. Lett. **112**, 23503 (2018).

[13] S.J. Pearton, F. Ren, M. Tadjer, and J. Kim, J. Appl. Phys. **124**, 220901 (2018).

[14] A. Kyrtsos, M. Matsubara, and E. Bellotti, Appl. Phys. Lett. **112**, 32108 (2018).

[15] X. Zhou, Q. Liu, W. Hao, G. Xu, and S. Long, Proc. Int. Symp. Power Semicond. Devices ICs **2022-May**, 101 (2022).

[16] C. Wang, H. Gong, W. Lei, Y. Cai, Z. Hu, S. Xu, Z. Liu, Q. Feng, H. Zhou, J. Ye, J. Zhang, R. Zhang, and Y. Hao, IEEE Electron Device Lett. **42**, 485 (2021).

[17] F. Zhou, H. Gong, M. Xiao, Y. Ma, Z. Wang, X. Yu, L. Li, L. Fu, H.H. Tan, Y. Yang, F.-F. Ren, S. Gu, Y. Zheng, H. Lu, R. Zhang, Y. Zhang, and J. Ye, Nat. Commun. **14**, 4459 (2023).

[18] Z. Wang, H. Gong, C. Meng, X. Yu, X. Sun, C. Zhang, X. Ji, F. Ren, S. Gu, Y. Zheng, R. Zhang, and J. Ye, IEEE Trans. Electron Devices **69**, 981 (2022).

[19] Z. Wang, H.-H. Gong, X.-X. Yu, X. Ji, F.-F. Ren, Y. Yang, S. Gu, Y. Zheng, R. Zhang, and J. Ye, Sci. China Mater. **66**, 1157 (2023).

[20] H. Gong, X. Chen, Y. Xu, Y. Chen, F. Ren, B. Liu, S. Gu, R. Zhang, and J. Ye, IEEE Trans. Electron Devices **67**, 3341 (2020).

[21] Z.P. Wang, H.H. Gong, X.X. Yu, T.C. Hu, X.L. Ji, F.-F. Ren, S.L. Gu, Y.D. Zheng, R. Zhang, and J.D. Ye, Appl. Phys. Lett. **122**, 152102 (2023).

[22] M. Labed, J.H. Park, A. Meftah, N. Sengouga, J.Y. Hong, Y.-K. Jung, and Y.S. Rim, ACS Appl. Electron. Mater. **3**, 3667 (2021).

[23] Rhoderick and williams, *Metal-Semiconductor Contacts* (n.d.).

[24] A.Y. Polyakov, N.B. Smirnov, I. V Shchemerov, S.J. Pearton, F. Ren, A. V Chernykh, P.B. Lagov, and T. V Kulevoy, APL Mater. **6**, 96102 (2018).

[25] K. Kanegae, M. Horita, T. Kimoto, and J. Suda, Appl. Phys. Express **11**, 71002 (2018).

[26] M. Aziz, J.F. Felix, N. Al Saqri, D. Jameel, F.S.A. Mashary, H.M. Albalawi, H.M.A.

Alghamdi, D. Taylor, and M. Henini, IEEE Trans. Electron Devices **62**, 3980 (2015).

[27] J. Zhang, P. Dong, K. Dang, Y. Zhang, Q. Yan, H. Xiang, J. Su, Z. Liu, M. Si, J. Gao, M. Kong, H. Zhou, and Y. Hao, Nat. Commun. **13**, 3900 (2022).

TABLE I: Summary of trap parameters extracted from DLTS and by considering the lambda effect for NiO/β-Ga_2O_3 HJ and Ni/β-Ga_2O_3 SBD.

Samples	E_T (eV)	Trap concentration N_t (cm^{-3})	Trap concentration $\widetilde{N_t}$ (cm^{-3})	Capture cross section $\sigma_{n,p}$ (cm^2)
SBD at V_R=-1 V	Ec-0.14 ±0.013 (E_SBD1)	2.35×10^{12}	4.85×10^{12}	1.30×10^{-18}
	Ec-0.33 ±0.10 (E_SBD2)	4.08×10^{13}	8.36×10^{13}	1.35×10^{-19}
HJ at V_R=-1 V	Ev+0.11 ±0.01 (H1)	2.79×10^{13}	6.12×10^{13}	1.07×10^{-14}
	Ec-0.77 ±0.2 (E2)	3.48×10^{13}	7.17×10^{13}	7.45×10^{-13}
SBD at V_R=-4 V	Ec-0.066 ±0.006 (E_SBD4)	6.07×10^{14}	9.17×10^{14}	7.57×10^{-21}

	Ec-0.24 ±0.01 (E_SBD5)	8.19×10^{13}	1.24×10^{14}	7.70×10^{-21}
HJ at V_R=-4 V	Ec-0.021 ±0.06 (H6)	3.97×10^{13}	5.99×10^{13}	9.91×10^{-21}
	Ec-0.036 ±0.001 (E7)	2.28×10^{14}	1.51×10^{14}	5.82×10^{-21}
	Ec-0.18 ±0.2 (E8)	1.49×10^{14}	2.25×10^{14}	9.98×10^{-21}

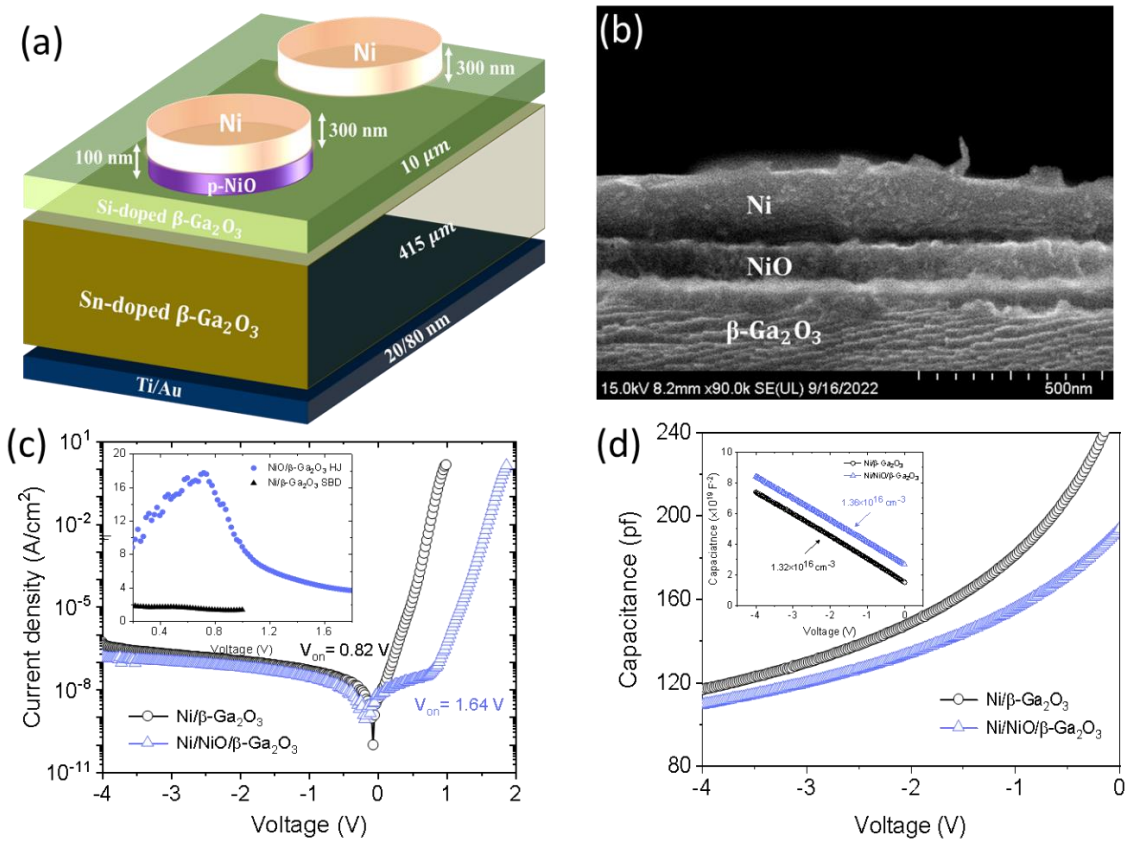

Figure 1: (a) Schematic of Ni/β-Ga_2O_3 SBD and NiO/β-Ga_2O_3 HJ devices, (b) SEM image of NiO/β-Ga_2O_3 HJ, (c) Semi-logarithmic J–V characteristics of NiO/β-Ga_2O_3 SBD and NiO/β-

Ga_2O_3 HJ, and the inset shows the extracted ideality factor vs forward bias for both devices and (d) C-V characteristics of both devices and the inset is the related $1/C^2$ versus reverse bias curves

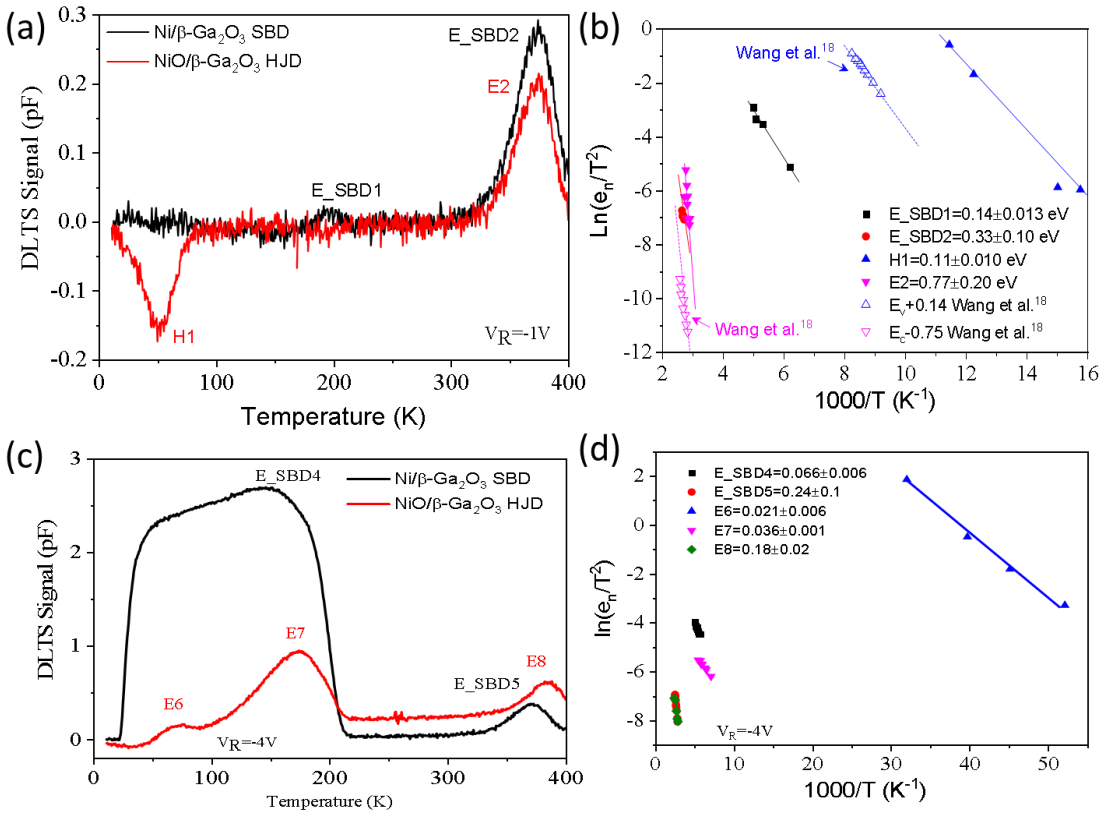

Figure 2: DLTS spectra of Ni/β-Ga_2O_3 SBD and NiO/β-Ga_2O_3 HJ at (a) V_R=-1 V, (c) V_R=-4V and (b) and (d) are Arrhenius plots of detected traps at V_R=-1 V and V_R=-4 V, respectively and the majority and minority trap levels reported previously for comparison purposes[18].

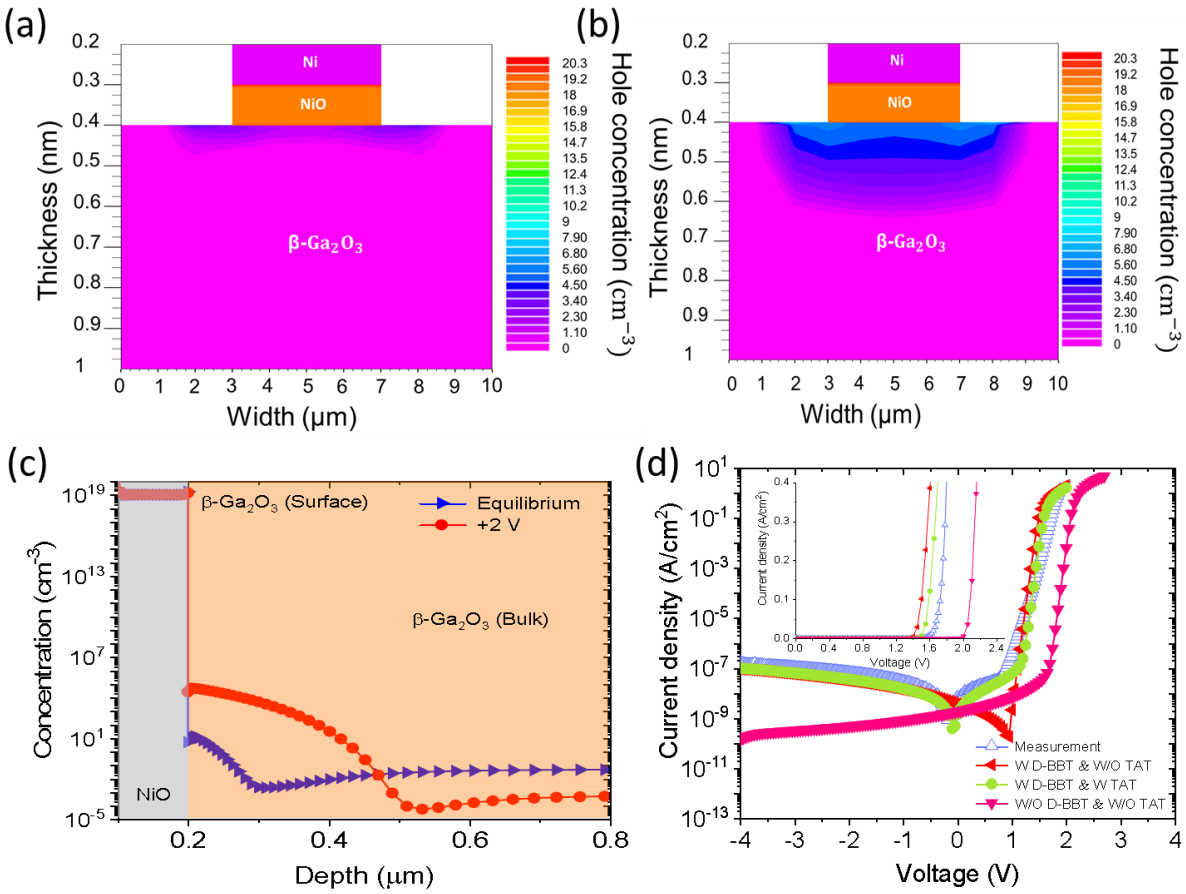

Figure 3: (a) and (b) Log_{10} scale of hole profile contour of NiO/β-Ga_2O_3 HJ at equilibrium and under +2 V forward voltage bias, respectively, (c) hole concentration profiles for NiO/β-Ga_2O_3 HJ at equilibrium and at a forward bias voltage of V=+2 V, and (d) comparison of semi-log current density versus bias voltage characteristics of simulated NiO/β-Ga_2O_3 HJ using different transport mechanisms and experiments. The inset shows the linear scale of the corresponding semi-logarithmic plots.